Spectroscopic Investigation of the Metal Coordination of the Aromatic Amino Acids with Zinc and Cadmium

Brandon C. Stevenson,[†] Giel Berden,[‡] Jonathan Martens,[‡] Jos Oomens,[‡,§] and P. B. Armentrout[†,]*

[†]Department of Chemistry, University of Utah, 315 South 1400 East, Room 2020, Salt Lake City, Utah 84112, USA

[‡]Radboud University, Institute for Molecules and Materials, FELIX Laboratory, Toernooiveld 7, 6525 ED Nijmegen, The Netherlands

[§]van't Hoff Institute for Molecular Sciences, University of Amsterdam, Science Park 904, NL-1098 XH Amsterdam, The Netherlands

* Corresponding author, e-mail: armentrout@chem.utah.edu

Abstract.

The aromatic amino acids (AAA), phenylalanine (Phe), tyrosine (Tyr), and tryptophan (Trp), were cationized with $ZnCl^+$ and $CdCl^+$ and the complexes evaluated using infrared multiple photon dissociation (IRMPD) action spectroscopy. Specifically, the $ZnCl^+$(Phe), $CdCl^+$(Phe), $ZnCl^+$(Tyr), $CdCl^+$(Tyr), and $ZnCl^+$(Trp) species were examined because the $CdCl^+$(Trp) IRMPD spectrum is available in the literature. Several low-energy conformers for all complexes were found using quantum chemical calculations and their simulated vibrational spectra were compared to the experimental IRMPD spectra to identify dominant isomers formed. In the case of MCl^+(Phe) and MCl^+(Tyr), these comparisons indicated the dominant binding motif is a tridentate structure where the metal atom coordinates with the backbone amino nitrogen and carbonyl oxygen, as well as the aryl ring. These observations are consistent with the predicted ground states at the B3LYP, B3P86, B3LYP-GD3BJ, and MP2 levels of theory. For the $ZnCl^+$(Trp) system, the experimental spectrum indicates a similar binding motif, with the zinc atom coordinating with the backbone nitrogen and carbonyl oxygen and either the pyrrole ring or the benzene ring of the indole sidechain. These observations are consistent with the predicted low-lying conformers identified by the aforementioned levels of theory, with the B3LYP and B3P86 levels predicting the metal-pyrrole

ring interaction is more favorable than the metal-benzene ring interactions and the opposite at the B3LYP-GD3BJ and MP2 levels.

Introduction

Aromatic amino acids (AAA), phenylalanine (Phe), tyrosine (Tyr), and tryptophan (Trp), play an important biological role. In zinc finger proteins, Phe is likely responsible for increasing the thermodynamic stability of the folded form of the domain because of its hydrophobicity. Replacement of the Phe residue in such proteins with alanine results in a folding-free-energy change of 6.3 kJ/mol and an over ten-fold decrease in metal-ion affinity.[1] The body utilizes Tyr and Phe to produce signaling molecules such as thyroxine, dopamine, and adrenaline.[2] Trp is involved in the function of some ion channels, such as the gating of Ca^{2+} in N-methyl-d-aspartate (NDMA) receptors.[3]

There is a continued interest in the study of fundamental metal ion-amino acid coordination and their structural characteristics. Earlier spectroscopic studies have examined the metal cationized amino acids in the following systems: histidine (His)[4, 5] and histidine dimer (His-H)(His),[6, 7] cysteine (Cys) and cysteine methyl ester (Cys-OMe),[8, 9] glutamine (Gln),[10, 11] serine (Ser),[12, 13] asparagine (Asn),[14, 15] glutamic acid (Glu),[16, 17] aspartic acid (Asp),[17, 18] arginine (Arg),[19-21] lysine (Lys),[22-24] threonine (Thr),[25, 26] proline (Pro),[27] valine (Val),[28] glycine (Gly),[29, 30] and methionine (Met).[31, 32] Several studies have also examined the interactions between the AAAs and alkali, alkaline earth, and transition metal cations.[33-35] In the present work, we extend these previous explorations to the assessment of the fundamental interactions between zinc or cadmium and the AAAs using infrared multiple photon dissociation (IRMPD) action spectroscopy. Zinc plays an important physiological role, while cadmium is an environmental pollutant that can replace the metal center in some zinc finger proteins.[36] Zinc and cadmium have fairly similar ionic radii (Zn^{2+}, 0.60 Å; Cd^{2+}, 0.78 Å),[37] and the same valence configuration (d^{10}) and oxidation state (+2).

Specifically, the $ZnCl^{+}$(Phe), $ZnCl^{+}$(Tyr), and $ZnCl^{+}$(Trp) complexes will be presented.

The analogous cadmium complexes, $CdCl^+$(Phe) and $CdCl^+$(Tyr), are also examined to ascertain the influence of metal ion character. The IRMPD spectrum of $CdCl^+$(Trp) has been previously reported elsewhere.[33] Elucidation of the binding character of these complexes was done by comparing the experimental action spectra with the vibrational spectra predicted by quantum-chemical calculations. Exploring differences in coordination between these two metals and the AAAs can lay the groundwork for understating physiological processes, as well as playing a role in the design of molecular ligands that selectively coordinate with transition metals. For both metal systems, the chloride ligand attached to the metal benefits this study in several ways. First, the systems considered here allow the metal ion to be in the +2 oxidation state while only carrying a +1 charge, making it a more realistic biomimetic complex.[33] Second, the chloride ligand can be thought of as a substitute for ligation with nearby residues in a biological system (see further discussion below). Third, chloride is utilized here as it is more biologically relevant than any of the other halides.

Interactions between these Group 12-containing systems differ from the classical cation-π interactions, which are typically interactions between Group 1 elements (namely potassium and sodium) and the aromatic amino acids. Typically, cation-π coordination arises from the electrostatic interactions involving the polarizability and quadrupole charge distribution of the aromatic π system. Here, the Zn^{2+} and Cd^{2+} ions both have a d^{10} configuration, and like the Group 1 elemental cations, they can accept electron density in the empty valence s orbital; however, because they are formally doubly charged, the interactions with electron donors, including the aromatic π system should be enhanced. Therefore, this study complements previous work examining cation-π interactions.

Experimental and Computational Section

Mass Spectrometry and IRMPD Photodissociation

The subject cation complexes were irradiated with light from the FELIX beamline at the free-electron laser for infrared experiments (FELIX) facility at Radboud University, the

Netherlands.[38] The infrared action spectra of the Zn metallated species were collected using a 4.7 T Fourier transform ion cyclotron resonance (FTICR) mass spectrometer, detailed elsewhere.[34, 39, 40] The Cd species were acquired using a quadrupole ion trap (QIT) mass spectrometer (Bruker, Amazon Speed ETD) modified to allow optical access to the ion trap.[41] The use of two mass spectrometers to collect these action spectra was done to economize available beamtime. Although the properties of the MS platforms are quite different (especially the ESI source, ion trapping region, mass resolution, sensitivity, and dynamic range),[41-43] recent work on a similar system indicates that the conformations observed in either instrument are largely consistent with one another.[7]

Ions were generated by electrospray ionization from solutions containing ~1 mM metal chloride salt and aromatic amino acid in a 1:1 methanol-water mixture. For the FTICR experiments, this solution was directly used to produce the ions of interest. In the case of the QIT, this solution was further diluted 100 times into methanol before ionization. Reagents were obtained from commercial sources and used without any further purification. The metallated complexes were independently mass isolated and irradiated with two (for the QIT) or 7-10 (for the FTICR) macropulses from the free-electron laser (5 or 10 Hz macropulse repetition rate, up to 130 mJ per pulse, ~0.5% bandwidth of central frequency). In some cases, filters were inserted into the beamline to attenuate the power of the FEL light, in order to prevent excessive precursor ion depletion and/or formation of fragment ions below the low mass cut-off of the QIT. Infrared action spectra were generated by plotting the photofragmentation yield (Y) as a function of the laser frequency using the equation $Y = -\ln[\Sigma I_P / (\Sigma I_F + \Sigma I_P)]$, where the precursor ($I_P$) and fragment ($I_F$) ion mass peaks are the integrated intensities.[43] To account for frequency-dependent variations in the FEL power, a linear correction was applied to the yield.[43, 44]

Computational Details

All calculations utilized Gaussian16.[45] Starting with the zinc species, initial geometry optimizations used the B3LYP/6-31G(d) level of theory and the "loose" keyword to facilitate convergence. Distinctive geometries underwent a second geometry optimization at the B3LYP/6-

311+G(d,p) level of theory. From these structures, the Zn atom was replaced with Cd and reoptimized at the B3LYP/def2-TZVP level of theory, which included a small core (28 electron) effective core potential (ECP) on Cd. The def2-TZVP basis set and Cd ECP were obtained from the EMSL Basis Set Exchange.[46] From these optimized structures, vibrational frequencies were calculated at the same level used for their geometry optimization. For comparison to the experimental action spectra, vibrational frequencies were scaled by 0.975 and broadened using a Gaussian line shape (25 cm^{-1} FWHM).[47]

Subsequently, single-point energy (SPE) calculations were performed on the optimized geometries for both metallated species at the B3LYP, B3P86, and MP2(full) levels of theory using larger basis sets (Zn, 6-311+G(2d,2p); Cd def2-TZVPP). To obtain 0 K relative enthalpies and 298 K Gibbs energies, zero-point energy (ZPE) and thermal corrections were applied to SPEs using a factor of 0.9896 to scale the aforementioned vibrational frequencies.[48] Additionally, calculations were performed to investigate the effect of dispersion forces on the optimized geometries. Geometries and frequencies were reoptimized to include the B3LYP-GD3BJ empirical dispersion method again using the 6-311+G(d,p) or def2-TZVP basis sets.[49, 50] The above scaling factor (0.9896) was again used to provide 0 K relative enthalpies and 298 K Gibbs energies for the GB3BJ structures. The larger basis sets (Zn, 6-311+G(2d,2p); Cd, def2-TZVPP) were also used to calculate the B3LYP-GD3BJ SPEs. The above combination of functionals, basis sets, ECP, scaling factors, and the assumption that the ion populations are well-predicted by their relative energies at 298 K is consistent with previous work on similar systems.[4-10, 12-16, 18, 19, 24-26, 31, 32]

Results and Discussion

Nomenclature

To facilitate discussion about the identified complexes, the following naming system was used. The metal-binding sites are identified in square brackets (N = amino nitrogen, CO = carbonyl oxygen, OH = hydroxyl oxygen, π = aromatic ring [5π or 6π specified for Trp when referring to the pyrrole or benzene ring of the indole sidechain]). When two or more complexes share the same

name, the metal-binding site precedes a number in parentheses, that designates the energy order where the structure lowest in relative energy is left unnumbered. In the case of Trp, the metal binding site is followed by a subscripted *s* or *a*, differentiating between rotamers of the sidechain where the nitrogen of the pyrrole ring is closest (syn, *s*) to the amine nitrogen, or on the opposite side (anti, *a*).

Relative Energies and Structures of Phe Complexes

The calculated relative energies for the MCl^+(Phe) species are shown in Table 1. The lowest-lying structures are pictured in Figure 1. In the following discussion, values referenced will be those corrected to thermal temperatures, as the temperature of these ions is assumed to be roughly 298 K when irradiated in their respective instrument. The relative energies at 0 K can be found in the Supporting Information (Tables S1 – S3). At all four levels of theory used herein, the [N,CO,π] complex was identified as the ground structure (GS) for both metals. This structure is characterized by the metal atom coordinating with the amine nitrogen, carbonyl oxygen, and π ring of the phenylalanine ring. The Cl ligand is bound to the metal atom and, for all species studied here, moving the chloride ligand away from the metal atom always resulted in the geometry optimization bringing the two back together.

The species next highest in energy is the [N,CO] conformer, where the metal is no longer coordinating with the π ring. The dipole of the MCl^+ for this structure is oriented directly between the amino nitrogen and carbonyl oxygen. In contrast, the dipole for the MCl^+ in the GS is tilted such that the chlorine atom is pointing away from the phenyl ring, which appears to compromise the metal coordination with the amine nitrogen and carbonyl oxygen. Therefore, loss of the π-ring coordination and the shift in the MCl^+ dipole orientation results in only a small energetic penalty at the B3LYP level of theory for the zinc system, which places this structure less than 1 kJ/mol above the ground state. For $CdCl^+$(Phe), the [N,CO] conformer is only 4 kJ/mol higher in energy than the GS at the B3LYP level. This small difference between the two metal species could be a result of differences in the basis sets being used for each metal. In both metal species, MP2 and

B3LYP-GD3BJ levels both place much higher energetic penalties (Zn, 22 and 29 kJ/mol; Cd, 26 and 33 kJ/mol) on the loss of the π-ring coordination. B3P86 places a smaller penalty (Zn, 9 kJ/mol; Cd, 11 kJ/mol), closer to that predicted by B3LYP. A second [N,CO] structure was also located, [N,CO] (2), which orients the amino acid backbone such that the carboxylic acid group is now closer to the aromatic sidechain. Such an orientation carries a relative energetic penalty of ~ 14 kJ/mol relative to that of the [N,CO] conformation, where the amine group is oriented closer to the aromatic sidechain.

Next highest in energy is the [N, π] conformer. The metal is bound to the amine nitrogen and the π ring. The lack of carbonyl coordination has a significant predicted energetic penalty at all levels of theory (19 – 29 kJ/mol). Above that conformation, two [CO,π] structures were located and differ in the dihedral angle of the carboxylic acid proton. The lower energy [CO,π] coordination orients the carboxylic acid hydrogen such that it forms a stabilizing hydrogen bond with the amine group. Highest in energy of the explored structures is the [CO] conformation, where the metal coordinates to a single carboxylic oxygen, which is predicted to be 96 – 147 kJ/mol higher in energy than the tridentate GS.

Relative Energies and Structures of Tyr Complexes

The calculated relative energies for the MCl^+(Tyr) species are shown in Table 2. The energetic orderings of these species are largely consistent with those observed for Phe. The phenolic OH-group was not observed to contribute to metal coordination and all starting structures that involved said group coordinating with the metal atom collapsed to structures that favored other binding sites. Rotation of the phenolic OH did not change the calculated energies noticeably (< 1 kJ/mol), but for consistency, all energies reported had the hydrogen pointing towards the amine group. This minimal change in energy is consistent with previous explorations of metallated Tyr.[51] Because of this, all structures are directly analogous with those shown in Figure 1 for Phe. Here, all four levels of theory identified the [N,CO,π] complex as the GS for both the Zn and Cd species. Similarly, the [N,CO] and [N, π] structures were found to be the next two structures higher in energy.

Relative Energies and Structures of the Trp Complex

Table 3 shows the predicted relative energies for $ZnCl^+$(Trp) conformers, and select conformations are shown in Figure 2. Here, the GS was determined to be $[N,CO,5\pi]_a$, where the metal cation is bound to the amine nitrogen, the carbonyl oxygen, and the pyrrole ring of the indole sidechain, Figure 2. Because of the asymmetrical nature of the indole sidechain, the $[N,CO,5\pi]_s$ rotamer was also explored. The binding of the rotamer is the same as the GS but the indole sidechain is rotated, Figure 2. All levels of theory place this structure approximately 2 kJ/mol higher in energy than the GS.

Above the $[N,CO,5\pi]_a$ isomer, the $[N,CO,6\pi]_s$ conformer was identified, Figure 2. Shifting the metal coordination site from the pyrrole ring to the benzene ring is predicted to have an energetic penalty of 3 – 15 kJ/mol. This result contrasts with the traditionally studied cation (alkali metal) – π systems, where in low-energy structures, the significant positive charge on the pyrrole nitrogen shifts the metal ion away as far as possible without losing the benefit of the π system coordination.[52] In a theoretical study of the complexation of Na^+ with the aromatic amino acids, the ground structure for the Na^+(Trp) complex was found to be the $[N,CO,6\pi]_s$ conformer, with the $[N,CO,5\pi]_s$ conformer having a predicted energetic penalty of ~11 kJ/mol.[52] The specificity of Na^+ ion channels is theorized to be a result of binding Na^+ to exposed aromatic amino acid π systems, and this minor difference between the binding of Zn and Na may contribute to this specificity.[53, 54]

Several other conformers for both complexes were identified and their relative energies are presented in Table 3. In all cases, it is worth noting that the relative orientation of the Trp sidechain did influence the predicted relative energetics, but did not systematically favor either the *syn* or *anti* orientation. Additionally, different levels of theory predict different energetic penalties for these sidechain orientations.

The analogous Cd complexes were also calculated for comparison, Table 3. There, the $[N,CO,5\pi]_a$ was also identified as the GS at the B3LYP and B3P86 levels of theory, whereas the $[N,CO,6\pi]_a$ was found to be the GS at the MP2 level. For B3LYP-GD3BJ, the $[N,CO,5\pi]_a$

geometry collapsed to the $[N,CO,6\pi]_a$ geometry during the B3LYP-GD3BJ reoptimization, potentially indicating that even a system as simple as a metallated peptide is subject to dispersion forces that influence the optimized geometry.

Barriers for Interconversion at Room Temperature

As suggested by a referee, we examined barriers for interconversion between the lowest-lying complexes for $ZnCl^+$(Phe) and $ZnCl^+$(Trp), as several conformations may be energetically competitive at thermal energies. The Tyr complex was not investigated as it is likely to parallel the Phe results. In the case of $ZnCl^+$(Phe), a transition state (TS) complex was located that bridged the [N,CO,π] and [N,CO] structures. This complex is calculated to sit 17 – 40 kJ/mol above the GS, indicating that interconversion between these tri- and bidentate Phe complexes is inaccessible at room temperature. In the case of $ZnCl^+$(Trp), a TS was located between $[N,CO,5\pi]_a$ and $[N,CO,6\pi]_a$. The 298 K Gibbs energies place this structure 8 – 13 kJ/mol above the $[N,CO,5\pi]_a$ GS, which makes it unlikely that the $[N,CO,5\pi]_a$ converts into the $[N,CO,6\pi]_a$ structure without the input of energy in excess of that available to these room temperature ions. From the perspective of the $[N,CO,6\pi]_a$ structure, the TS is predicted to be 3 – 7 kJ/mol higher in energy using the DFT methods. The MP2 calculation places this TS 4 kJ/mol below that of the $[N,CO,6\pi]_a$ structure, indicating that this structure would not be observed and would instead collapse to the $[N,CO,5\pi]_a$ structure.

IRMPD Spectra of Metallated Aromatic Amino Acids

Infrared multiple photon dissociation spectra of all five metallated amino acid species, $ZnCl(Phe)^+$, $ZnCl(Tyr)^+$, $ZnCl(Trp)^+$, $CdCl(Phe)^+$ and $CdCl(Tyr)^+$, are compared in Figure 3. Both the Phe and Tyr species share several of the same bands, potentially indicating that both Zn and Cd metallated systems share a similar binding motif, as supported by the discussion of the theoretical structures above. The spectra for the $CdCl^+$(Phe) and $CdCl^+$(Tyr) species (taken on the QIT mass spectrometer) required the full laser pulse energy to observe bands below 1000 cm^{-1}, whereas only 30 – 50% of the laser energy was required to observe bands above 1000 cm^{-1}. The Zn species were collected on the FTICR mass spectrometer, which has a lower operating pressure

inside the ion trap, reducing the effects of collisional cooling on the IRMPD process. Thus, the FTICR could be used to acquire the total spectrum using a single attenuation of the FEL. In the case of Trp, the analogous $CdCl^+$(Trp) species has been published elsewhere,[33] but similar bands for both species are apparent. Here, we also extended the range of the spectra collected from a lower limit of ~700 cm^{-1} to ~590 cm^{-1}, facilitating the collection of an additional band centered at 630 cm^{-1}. The fragment ions used to generate the IRMPD spectra are tabulated in the Supporting Information (Table S4). Wavelength-dependent fragmentation patterns for each fragment were individually inspected to ensure they match with the overall yield spectrum measured for each species. The baseline of the IRMPD spectra was also magnified by a factor of ten to ensure that no small bands were missed.

Comparison of Experimental and Theoretical Spectra: MCl^+(Phe)

Figure 4 shows the experimental IRMPD spectrum for MCl^+(Phe) compared to the calculated spectra for the three lowest-lying conformers for each metal. For the Zn species, bands are located at 1680, 1581, 1447, 1169, 1065, 739, 709, and 630 cm^{-1}. The GS conformation, [N,CO,π], replicates all these experimental features. In detail, vibrational bands are predicted at 1678 (coordinated CO stretch); 1610 (NH_2 scissor); 1429 (C-OH stretch and NH_2 twist); 1179 (COH bend); 1069 (NH_2 wag); 771, 737, 709 (CH backbone and benzene ring motions); and 650 cm^{-1} (COH out-of-plane bend and NH_2 twist). As discussed elsewhere,[4-10, 12-14, 16, 26] the NH_2 scissoring motion at 1610 cm^{-1} can be strongly anharmonic, which explains its deviation from the experimental band by almost 30 cm^{-1}.

The [N,CO] complex for Zn is also compared to the experimental IRMPD spectrum in Figure 4. Here, the bands predicted at 1657, 1614, 1433, and 1184 cm^{-1} are close to those predicted for the [N,CO,π] structure; however, the coordinated CO stretch is red-shifted by ~20 cm^{-1}, and as such, does not match the experimental spectrum as well as [N,CO,π]. The largest deviation from experiment comes from the NH_2 wagging motion, which is predicted at 1069 cm^{-1} in the [N,CO,π] structure but is now blue-shifted to 1147 cm^{-1}. This shift is likely a result of the $ZnCl^+$ binding more tightly with the carboxylic oxygen and amine nitrogen, which is reflected in the shortened

bond length between the metal and the coordination sites when compared to the [N,CO,π] structure. Experimentally, there is no evidence for this band at the predicted location, suggesting that this structure is not a major contributor to the experimental spectrum, but could be present in small amounts.

Finally, the [N,π] simulated spectrum is compared to the experimental IRMPD spectrum. The coordinated CO stretch is predicted to be at 1774, which is clearly inconsistent with the experimental peak at 1680 cm^{-1}. Overall, we conclude that the [N,CO,π] conformation is the dominant isomer present in the experimental spectrum of $ZnCl^+$(Phe), with minor contributions from the [N,CO] possible. At the B3LYP level of theory, a calculated equilibrium distribution at 298 K predicts 85% of the population adopts the [N,CO,π] conformation, with the remaining population in [N,CO]. All other levels of theory used here predict >99% of the ion population to be composed of the [N,CO,π] conformation, which agrees better with experiment. This result suggests that B3LYP is potentially underestimating the contribution of the π-ring coordination to the relative stability.

Figure 4 also shows the comparison between the $CdCl^+$(Phe) experimental action spectrum and the three lowest-lying structures. Experimental bands are centered at 1698, 1586, 1443, 1166, 1047, 739, 712, and 621 cm^{-1}. Again, the [N,CO,π] conformer is the best match to the experimental spectrum, with the most noticeable difference being that the [N,CO,π] does not recreate the narrow and relatively intense experimental band at 621 cm^{-1}. The [N,CO] conformer does a fair job of recreating many bands, but predicts a band at 1119 cm^{-1} (NH_2 wag), for which there is no experimental evidence. For the [N,π] conformation, this structure does a fair job of recreating the low-frequency experimental bands, but does not predict the high wavenumber bands. We therefore conclude that the $CdCl^+$(Phe) is composed entirely of the [N,CO,π] conformation. This conclusion agrees with theoretically predicted distributions at 298 K.

Comparison of Experimental and Theoretical Spectra: MCl^+(Tyr)

Figure 5 compares the experimental action spectrum of $ZnCl^+$(Tyr) with predicted spectra for the three lowest-lying species. Experimental bands are found at 1685, 1585, 1504, 1449, 1283,

1168, 1059, 847, and 637 cm^{-1}, with possible shoulders at 1103 and 1328 cm^{-1}. Here, the [N,CO,π] GS conformation predicts all of these bands. Bands are predicted at 1681 (coordinated CO stretch); 1614 (NH_2 scissor); 1600 (CC stretches in the aromatic ring); 1503 (CH in-plane bend of the aromatic ring); 1428 (COH bend with contributions from asymmetric aromatic ring CH bends); 1335, 1325 (backbone CH motions); 1292 (CO stretch of the phenol); 1179 (COH in-plane bend); 1158 (COH in-plane bend of the phenol); 1105 (CH and OH bends of the sidechain); 1065 (NH_2 wag); 833 (CH out-of-plane bends of the aromatic ring); and 651 cm^{-1} (COH out-of-plane bend and NH_2 twist).

The [N,CO] complex is also compared to the experimental action complex, Figure 5. The predicted bands at 1655 and 1612/1607 cm^{-1} are blue- and red- shifted (respectively) relative to the experimental bands, leading to a qualitatively worse match when compared to the GS spectrum. The experimental band at 1059 cm^{-1} is also not meaningfully present in the [N,CO] spectrum. The [N,π] spectrum, also shown in Figure 5, shows significant deviations from the experimental spectrum (CO stretch is red shifted and it does not predict several experimental bands). We therefore conclude that the [N,CO,π] structure is the conformation present in the gas phase, but very minor contributions from the [N,CO] structure cannot be excluded as those bands may be obscured by the more intense bands attributed to the [N,CO,π] structure. This conclusion is consistent with the ion population predictions from the B3LYP-GD3BJ, B3P86, and MP2 levels of theory. B3LYP predicts 19% of the population would adopt the [N,CO] conformation.

Figure 5 also shows the $CdCl^+$(Tyr) action spectrum compared to the simulated spectra of low-energy structures. Here, experimental bands are found at 1699, 1585, 1504, 1440, 1290, 1160, 1042, 841, and 623 cm^{-1}. The simulated spectrum of [N,CO,π] recreates the experimental spectrum with excellent fidelity for even the low-intensity band centered at 1104 cm^{-1} and the shoulder at 1329 cm^{-1}. Theoretical bands are located at 1696, 1609, 1603, 1510, 1422, 1337, 1328, 1294, 1171, 1158, 1107, 1051, 838, and 633 cm^{-1} (band assignments are the same as the Zn species discussed above). The assignment of the dominant species being the [N,CO,π] conformation for the $CdCl^+$(Tyr) complex is also made here, as the simulated spectra for the higher-energy species are

poorer matches for the experimental spectrum. The [N,CO] structure cannot be eliminated from consideration on the basis of spectral analysis alone, but if present, makes up a small fraction of the total ion population. This conclusion also matches the population distributions predicted at 298 K by all levels of theory.

Comparison of Experimental and Theoretical Spectra: $ZnCl^+$(Trp)

Figure 6 compares the experimental IRMPD spectrum for $ZnCl^+$(Trp) compared with simulated spectra for several low-lying structures. Experimental features are centered at 1693, 1589, 1449, 1408, 1163, 1050, 744, and 640 cm^{-1}. The $[N,CO,5\pi]_a$ GS conformation has predicted bands at 1687 (coordinated CO stretch); 1614 (NH_2 scissor); 1429, 1405 (CH backbone and sidechain motions); 1180, 1174 (COH in-plane bend and CH backbone motions); 1057 (NH_2 wag); 742 (CH out-of-plane bends of the aromatic ring); and 652 cm^{-1} (COH out-of-plane bend and NH_2 twist). The simulated vibrational spectrum for the GS rotamer, $[N,CO,5\pi]_s$, is also shown in Figure 6. Only minor differences in relative band intensities are visible between the *anti* and *syn* rotamers, and there is no clear diagnostic band to differentiate between these structures. This is the case for all rotamers studied here and as such, only the *syn* structures will be further compared to the experimental spectrum.

Figure 6 also compares the experimental action spectra with the [N,CO,6π] structure. As the binding character is very similar to the GS, the majority of the bands are similar, with a few distinct differences. First, although the NH_2 scissor motion predicted at 1594 cm^{-1} matches the experimental band at 1589 cm^{-1}, this band is routinely red-shifted compared to experiment (as noted above) such that this close match to the experimental band is suspect. Second, the [N,CO,6π] predicts a band at 1419 cm^{-1} that does not capture the doublet of experimental bands observed at 1449 and 1408 cm^{-1}. Finally, the experimental spectrum appears to have only a single band at both 744 and 640 cm^{-1}, whereas the simulated [N,CO,6π] spectrum predicts two bands at approximately those frequencies. There appears to be a slight shoulder (centered at 1108 cm^{-1}) on the 1050 cm^{-1} band, which could correlate to the small predicted band at 1077 cm^{-1}; however, the $[N,CO,5\pi]_a$

structure does predict a small band at 1108 cm^{-1}, but the predicted intensity is much lower than that of the experimental shoulder.

The $[N,6\pi]_s$ structure is also compared with the experimental spectrum in Figure 6. The [N,6π] spectrum has an extremely blue-shifted CO stretch predicted at 1770 cm^{-1}. Coupled with the energetic penalty that all four levels of theory place on this structure relative to the GS, we eliminate this structure from further consideration. Given the marked similarities in the predicted vibrational spectra for the [N,CO,6π] and [N,CO,5π], it is difficult to exclude the [N,CO,6π] structure from contributing to the gas-phase conformer population; however, as is clear from Figure 6, the [N,CO,5π] structures (either rotamer with the *anti* predicted to be lower in energy) are a better match to the experimental spectrum. Therefore, we conclude that the majority of the conformer population adopts the [N,CO,5π] structures, but cannot exclude contributions from the [N,CO,6π] conformers. The B3LYP and B3P86 levels of theory predict ~95% of the ion population to be in the [N,CO,5π] conformations, with the remaining in the [N,CO,6π]; whereas the B3LYP-GD3BJ level predicts a 1 : 3 ratio of the aforementioned structures. MP2 predicts the [N,CO,5π] structure to be exclusively present. Here, the observed spectrum more closely mirrors those predicted by B3LYP, B3P86, and MP2 levels of theory.

Comparison to Previous Studies

The $CdCl(Trp)^+$ IRMPD spectrum was presented previously,[33] and assigned to the $[N,CO,6\pi]_a$ geometry, which was found to be the lowest-lying structure at the B3LYP/6-31+G(d,p) level of theory (using the SDD basis set with ECP for Cd). Here, the same structure was also identified as the GS for the B3LYP-GD3BJ and MP2 levels of theory, whereas the B3LYP and B3P86 levels predicted the $[N,CO,5\pi]_a$ structure (which was not considered previously) is the GS, Table 3. All four levels of theory place these two structures within 2 kJ/mol of one another, although $[N,CO,5\pi]_a$ collapses to $[N,CO,6\pi]_a$ at the B3LYP-GD3BJ level. Comparing the spectra of $ZnCl^+$(Trp) obtained here with that published for $CdCl^+$(Tyr), all major bands appear in both experiments, with the exception that the $ZnCl^+$(Trp) band at 630 cm^{-1} was not observed for $CdCl^+$(Trp) because the experiment extended only to 700 cm^{-1}. Comparatively,

the shoulder feature seen at ~1100 cm^{-1} in the $ZnCl^+$(Trp) spectrum is more clearly resolved in the $CdCl^+$(Trp) spectrum.

Figure 7 presents a comparison between the previously recorded $CdCl(Trp)^+$ IRMPD spectrum[33] and the two lowest-lying structures identified here. Experimental bands are located at 1721, 1597, 1460, 1423, 1163, 1040, and 742 cm^{-1}. Both the $[N,CO,5\pi]_a$ and $[N,CO,6\pi]_a$ recreate the majority of the experimental bands, with some small band shape differences. The simulated spectrum of $[N,CO,5\pi]_a$ predicts bands at 1701, 1609, 1422, 1406, 1172, 1160, 1034, 743, and 641 cm^{-1} and the $[N,CO,6\pi]_a$ has predicted bands at 1707, 1610, 1418, 1410, 1176, 1152, 1067, 738, and 620 cm^{-1} (band assignments are the same as the Zn species). The width of the experimental band centered at 1040 cm^{-1} is consistent with NH_2 wagging predicted bands from *both* the 5π and 6π conformer, 1034 and 1067 cm^{-1}, respectively. In the 5π conformer, the amine nitrogen sits closer to the tryptophan sidechain, in comparison to the 6π conformer, to facilitate the metal—pyrrole ring coordination. This change in local environment explains the 33 cm^{-1} shift of the NH_2 wagging motion predicted for these conformers. As with $ZnCl^+$(Trp), we conclude that both the [N,CO,5π] and [N,CO,6π] structures probably contribute to the observed spectrum. B3LYP and B3P86 predict the $CdCl(Trp)^+$ $[N,CO,5\pi]_a$ geometry makes up 66% of the ion population at 298 K, whereas MP2 predicts the $[N,CO,6\pi]_a$ geometry makes up 68% of the conformation population and B3LYP-GD3BJ, 100%.

Both monomeric and dimeric forms of the metallated AAAs have been the focus of several studies, the earliest of which studied monomeric phenylalanine complexed with silver (Ag^+).[34] The Ag^+(Phe) species was found to adopt a tridentate chelation, [N,CO,π], as was shown here for the analogous Phe and Tyr complexes. In the same study, the $Zn(Phe\text{-}H)(Phe)^+$ species was found to adopt a hexadentate chelation through the amine nitrogens, carbonyl oxygens, and aromatic rings of both of Phe ligands, i.e., the $[N,CO^-,\pi][N,CO,\pi]$ conformer. This complexation of Zn with the intact Phe ligand mirrors that observed here for $ZnCl^+$(Phe), which indicates that although the Cl ligand used in the present study is almost certainly altering the electron density of the Zn metal, these effects are not strong enough to induce a different coordination motif. To further explore the

effect of the Cl ligand on the remaining two AAAs, we have also collected IRMPD spectra for $[Zn^{2+}(Trp\text{-}H)(Trp)]^+$ and $[Zn^{2+}(Tyr\text{-}H)(Tyr)]^+$, which will be published in an upcoming publication. Preliminary results indicate that the metal – intact coordinating ligand (Tyr or Trp) mirrors that of the dominant conformations identified here, signaling again that the Cl ligand is providing a reasonable mimic for any anionic ligand.

More recently, a systematic study of metal cation size and charge was conducted with Phe,[35] and showed that for small, singly charged ions (Li^+, Na^+, K^+, Ag^+), the dominant conformation was the aforementioned tridentate chelation. The larger alkali cations (Rb^+, Cs^+), adopt a similar [N,CO,π] tridentate conformation but a noticeable fraction of the ion population adopts a [CO,π] bidentate conformation, coordinating with the carboxylic oxygen and aromatic ring. Experimentally, the Zn and Cd complexes with Phe presented here are clearly coordinated in a tridentate fashion, indicating their metal character is closer to that of the smaller alkalis than that of the larger alkalis. This result appears to be driven by the higher charge density on these cations.

One could wonder whether the relative energies of these complexes would change with solvation. Remko et al.[55] have investigated this question for Zn^{2+}(AAA) systems and found that, in the absence of water molecules, the most stable structure they located had Zn^{2+} coordinated with the amine nitrogen and aromatic sidechain, which is consistent with the [N,π] structure located here. In the cases of Phe and Trp, the addition of water molecules shifts the relative stability of these structures to favor [N,CO] coordination, presumably because the water binds to the metal cation more strongly than to the aromatic ring. Tyr, on the other hand, exhibits no shift, and the global minima remains [N,π].

In the study of Remko et al., the tridentate conformation was not considered, most likely because such a structure can only be optimized in the absence of water molecules (as confirmed by some preliminary calculations performed here). In the case of $ZnCl^+$(Phe), when the tridentate GS structure is optimized in the presence of a polarizable continuum model (PCM),[56, 57] which is an implicit solvation model (using the keywords, "SCRF=(PCM, solvent=water)"), the $ZnCl^+$ shifts away from the π system and resembles the [N,CO] structure. This is most likely because the

solvation of MCl^+ is favored relative to the MCl^+ — π interaction. Thus, the solvation of these ions plays a significant role in the adopted structures and indicates that the GS conformations identified here may only be significantly populated when these ions are isolated in the gas phase.

Conclusions

The IRMPD action spectra of $ZnCl^+$(Phe), $CdCl^+$(Phe), $ZnCl^+$(Tyr), $CdCl^+$(Tyr), and $ZnCl^+$(Trp) were recorded from 600 – 1800 cm^{-1}, and were compared to simulated linear absorption IR spectra calculated at the B3LYP/6-311+G(d,p) level for Zn and B3LYP/def2-TZVP level for Cd. Excellent agreement between the GS conformations calculated at four levels of theory (B3LYP, B3LYP-GD3BJ, B3P86, and MP2) and the experimental spectra were found. In all cases, the metal-chloride complex was found to bind to the amine nitrogen, carbonyl oxygen, and the aromatic ring. In the case of Trp, the GS prefers coordination of the metal atom with the pyrrole ring of the indole sidechain. This structure is consistent with the experimental spectrum, but the structure where the metal atom coordinates with the phenyl ring also provides a reasonable match.

Supporting Information

Calculated relative Gibbs energies at 0 K for MCl^+(Phe), Table S1, MCl^+(Tyr), Table S2, and MCl^+(Trp), Table S3, where M = Zn and Cd. The fragment ions used to generate the IRMPD spectra are tabulated in Table S4.

Acknowledgments

Financial support for this work was provided by the National Science Foundation, Grants CHE-1954142. The authors gratefully acknowledge the *Nederlandse Organisatie voor Wetenschappelijk Onderzoek* (NWO) for the support of the FELIX Laboratory. We also appreciate a generous grant of computer time from the Center of High Performance Computing at the University of Utah.

References

1. Kilfoil, V. J. Structural Studies of a Consensus Zinc Finger Peptide and Variants by Nuclear Magnetic Resonance Spectroscopy. Johns Hopkins University, 1993.
2. Parthasarathy, A.; Cross, P. J.; Dobson, R. C.; Adams, L. E.; Savka, M. A.; Hudson, A. O. A Three-ring Circus: Metabolism of the Three Proteogenic Aromatic Amino Acids and Their Role in the Health of Plants and Animals. *Frontiers Molec. Biosci.* **2018,** *5*, 29.
3. Buck, D.; Howitt, S.; Clements, J. D. NMDA Channel Gating is Influenced by a Tryptophan Residue in the M2 Domain but Calcium Permeation is Not Altered. *Biophys. J.* **2000,** *79*, 2454-2462.
4. Hofstetter, T. E.; Howder, C.; Berden, G.; Oomens, J.; Armentrout, P. B. Structural Elucidation of Biological and Toxicological Complexes: Investigation of Monomeric and Dimeric Complexes of Histidine with Multiply Charged Transition Metal (Zn and Cd) Cations using IR Action Spectroscopy. *J. Phys. Chem. B* **2011,** *115*, 12648-12661.
5. Citir, M.; Hinton, C. S.; Oomens, J.; Steill, J. D.; Armentrout, P. B. Infrared Multiple Photon Dissociation Spectroscopy of Cationized Histidine: Effects of Metal Cation Size on Gas-Phase Conformation. *J. Phys. Chem. A* **2012,** *116*, 1532-1541.
6. Stevenson, B. C.; Martens, J.; Berden, G.; Oomens, J.; Schäfer, M.; Armentrout, P. B. IRMPD Spectroscopic and Theoretical Structural Investigations of Zinc and Cadmium Dications Bound to Histidine Dimers. *J. Phys. Chem. A* **2020,** *124*, 10266-10276.
7. Stevenson, B. C.; Peckelsen, K.; Martens, J.; Berden, G.; Oomens, J.; Schäfer, M.; Armentrout, P. B. An investigation of inter-ligand coordination and flexibility: IRMPD spectroscopic and theoretical evaluation of calcium and nickel histidine dimers. *J. Mol. Spectrosc.* **2021,** *381*, 111532.
8. Coates, R. A.; McNary, C. P.; Boles, G. C.; Berden, G.; Oomens, J.; Armentrout, P. B. Structural Characterization of Gas-Phase Cysteine and Cysteine Methyl Ester Complexes with Zinc and Cadmium Dications by Infrared Multiple Photon Dissociation Spectroscopy. *Phys. Chem. Chem. Phys.* **2015,** *17*, 25799-25808.
9. Citir, M.; Stennett, E. M. S.; Oomens, J.; Steill, J. D.; Rodgers, M. T.; Armentrout, P. B. Infrared Multiple Photon Dissociation Spectroscopy of Cationized Cysteine: Effects of Metal Cation Size on Gas-Phase Conformation. *Int. J. Mass Spectrom.* **2010,** *297*, 9-17.
10. Boles, G. C.; Coates, R. A.; Berden, G.; Oomens, J.; Armentrout, P. B. Experimental and Theoretical Investigations of Infrared Multiple Photon Dissociation Spectra of Glutamine Complexes with Zn^{2+} and Cd^{2+}. *J. Phys. Chem. B* **2015,** *119*, 11607–11617.
11. Bush, M. F.; Oomens, J.; Saykally, R. J.; Williams, E. R. Alkali Metal Ion Binding to Glutamine and Glutamine Derivatives Investigated by Infrared Action Spectroscopy and Theory. *J. Phys. Chem. A* **2008,** *112*, 8578-8584.
12. Coates, R. A.; Boles, G. C.; McNary, C. P.; Berden, G.; Oomens, J.; Armentrout, P. B. Zn^{2+} and Cd^{2+} Cationized Serine Complexes: Infrared Multiple Photon Dissociation Spectroscopy and Density Functional Theory Investigations. *Phys. Chem. Chem. Phys.* **2016,** *18*, 22434 – 22445.
13. Armentrout, P. B.; Rodgers, M. T.; Oomens, J.; Steill, J. D. Infrared Multiphoton Dissociation Spectroscopy of Cationized Serine: Effects of Alkali-Metal Cation Size on Gas-Phase Conformation. *J. Phys. Chem. A* **2008,** *112*, 2248-2257.
14. Boles, G. C.; Coates, R. A.; Berden, G.; Oomens, J.; Armentrout, P. B. Experimental and Theoretical Investigations of Infrared Multiple Photon Dissociation Spectra of Asparagine

Complexes with Zn^{2+} and Cd^{2+} and Their Deamidation Processes. *J. Phys. Chem. B* **2016,** *120*, 12486-12500.
15. Heaton, A. L.; Bowman, V. N.; Oomens, J.; Steill, J. D.; Armentrout, P. B. Infrared Multiple Photon Dissociation Spectroscopy of Cationized Asparagine: Effects of Metal Cation Size on Gas-Phase Conformation. *J. Phys. Chem. A* **2009,** *113*, 5519-5530.
16. Boles, G. C.; Owen, C. J.; Berden, G.; Oomens, J.; Armentrout, P. B. Experimental and Theoretical Investigations of Infrared Multiple Photon Dissociation Spectra of Glutamic Acid Complexes with Zn^{2+} and Cd^{2+}. *Phys. Chem. Chem. Phys.* **2017,** *19*, 12394 - 12406.
17. O'Brien, J. T.; Prell, J. S.; Steill, J. D.; Oomens, J.; Williams, E. R. Interactions of Mono- and Divalent Metal Ions with Aspartic and Glutamic Acid Investigated with IR Photodissociation Spectroscopy and Theory. *J. Phys. Chem. A* **2008,** *112*, 10823-10830.
18. Boles, G. C.; Hightower, R. L.; Coates, R. A.; McNary, C. P.; Berden, G.; Oomens, J.; Armentrout, P. B. Experimental and Theoretical Investigations of Infrared Multiple Photon Dissociation Spectra of Aspartic Acid Complexes with Zn^{2+} and Cd^{2+}. *J. Phys. Chem. B* **2018,** *122*, 3836-3853.
19. Chalifoux, A. M.; Boles, G. C.; Berden, G.; Oomens, J.; Armentrout, P. B. Experimental and Theoretical Investigations of Infrared Multiple Photon Dissociation Spectra of Arginine Complexes with Zn^{2+} and Cd^{2+}. *Phys. Chem. Chem. Phys.* **2018,** *20*, 20712-20725.
20. Bush, M. F.; O'Brien, J. T.; Prell, J. S.; Saykally, R. J.; Williams, E. R. Infrared Spectroscopy of Cationized Arginine in the Gas Phase: Direct Evidence for the Transition from Nonzwitterionic to Zwitterionic Structure. *J. Am. Chem. Soc.* **2007,** *129*, 1612-1622.
21. Forbes, M. W.; Bush, M. F.; Polfer, N. C.; Oomens, J.; Dunbar, R. C.; Williams, E. R.; Jockusch, R. A. Infrared Spectroscopy of Arginine Cation Complexes: Direct Observation of Gas-Phase Zwitterions. *J. Phys. Chem. A* **2007,** *111*, 11759-11770.
22. Bush, M. F.; Forbes, M. W.; Jockusch, R. A.; Oomens, J.; Polfer, N. C.; Saykally, R. J.; Williams, E. R. Infrared Spectroscopy of Cationized Lysine and ε-N-methyllysine in the Gas Phase: Effects of Alkali-Metal Ion Size and Proton Affinity on Zwitterion Stability. *J. Phys. Chem. A* **2007,** *111*, 7753-7760.
23. Bush, M. F.; Oomens, J.; Williams, E. R. Proton Affinity and Zwitterion Stability: New Results from Infrared Spectroscopy and Theory of Cationized Lysine and Analogues in the Gas Phase. *J. Phys. Chem. A* **2009,** *113*, 431-438.
24. Owen, C. J.; Boles, G. C.; Berden, G.; Oomens, J.; Armentrout, P. B. Experimental and Theoretical Investigations of Infrared Multiple Photon Dissociation Spectra of Lysine Complexes with Zn^{2+} and Cd^{2+}. *Eur. J. Mass Spectrom.* **2019,** *25*, 97-111.
25. Boles, G. C.; Hightower, R. L.; Berden, G.; Oomens, J.; Armentrout, P. B. Zinc and Cadmium Complexation of l-Threonine: An Infrared Multiple Photon Dissociation Spectroscopy and Theoretical Study. *J. Phys. Chem. B* **2019,** *123*, 9343-9354.
26. Rodgers, M. T.; Armentrout, P. B.; Oomens, J.; Steill, J. D. Infrared Multiphoton Dissociation Spectroscopy of Cationized Threonine: Effects of Alkali-Metal Cation Size on Gas-Phase Conformation. *J. Phys. Chem. A* **2008,** *112*, 2258-2267.
27. Drayss, M. K.; Blunk, D.; Oomens, J.; Schäfer, M. Infrared Multiple Photon Dissociation Spectroscopy of Potassiated Proline. *J. Phys Chem. A* **2008,** *112*, 11972-11974.
28. Bush, M. F.; Oomens, J.; Saykally, R. J.; Williams, E. R. Effects of Alkaline Earth Metal Ion Complexation on Amino Acid Zwitterion Stability: Results from Infrared Action Spectroscopy. *J. Am. Chem. Soc.* **2008,** *130*, 6463-6471.

29. Drayss, M. K.; Armentrout, P. B.; Oomens, J.; Schäfer, M. IR Spectroscopy of Cationized Aliphatic Amino Acids: Stability of Charge-solvated Structure Increases with Metal Cation Size. *Int. J. Mass Spectrom.* **2010,** *297*, 18–27.
30. Armentrout, P. B.; Stevenson, B. C.; Ghiassee, M.; Boles, G. C.; Berden, G.; Oomens, J. Infrared Multiple-photon Dissociation Spectroscopy of Cationized Glycine: Effects of Alkali Metal Cation Size on Gas-phase Conformation. *Phys. Chem. Chem. Phys.* **2022,** *24*, 22950-22959.
31. Boles, G. C.; Stevenson, B. C.; Hightower, R. L.; Berden, G.; Oomens, J.; Armentrout, P. B. Zinc and cadmium complexation of L-methionine: An infrared multiple photon dissociation spectroscopy and theoretical study. *J. Mass Spectrom.* **2021,** *56*, e4580.
32. Carl, D. R.; Cooper, T. E.; Oomens, J.; Steill, J. D.; Armentrout, P. B. Infrared Multiple Photon Dissociation Spectroscopy of Cationized Methionine: Effects of Alkali-Metal Cation Size on Gas-Phase Conformation. *Phys. Chem. Chem. Phys.* **2010,** *12*, 3384-3398.
33. Dunbar, R. C.; Steill, J. D.; Polfer, N. C.; Oomens, J. Dimeric Complexes of Tryptophan with M^{2+} Metal Ions. *J. Phys. Chem. A* **2009,** *113*, 845-851.
34. Polfer, N. C.; Oomens, J.; Moore, D. T.; von Helden, G.; Meijer, G.; Dunbar, R. C. Infrared Spectroscopy of Phenylalanine Ag(I) and Zn(II) Complexes in the Gas Phase. *J. Am. Chem. Soc.* **2006,** *128*, 517-525.
35. Dunbar, R. C.; Steill, J. D.; Oomens, J. Cationized phenylalanine conformations characterized by IRMPD and computation for singly and doubly charged ions. *Phys. Chem. Chem. Phys.* **2010,** *12*, 13383-13393.
36. Coleman, J. E. Zinc proteins: enzymes, storage proteins, transcription factors, and replication proteins. *Annu. Rev. Biochem.* **1992,** *61*, 897-946.
37. Shannon, R. D. Revised Effective Ionic Radii and Systematic Studies of Interatomic Distances in Halides and Chalcogenides. *Acta Cryst.* **1976,** *A32*, 751-767.
38. Oepts, D.; van der Meer, A. F. G.; van Amersfoort, P. W. The Free-Electron-Laser User Facility FELIX. *Infrared Phys. Technol.* **1995,** *36*, 297-308.
39. Valle, J. J.; Eyler, J. R.; Oomens, J.; Moore, D. T.; van der Meer, A. F. G.; von Heldon, G.; Meijer, G.; Hendrickson, C. L.; Marshall, A. G.; Blakney, G. T. Free Electron Laser-Fourier Transform Ion Cyclotron Resonance Mass Spectrometry Facility for Obtaining Infrared Multiphoton Dissociation Spectra of Gaseous Ions. *Rev. Sci. Instrum.* **2005,** *76*, 023103.
40. Polfer, N. C.; Oomens, J. Reaction products in mass spectrometry elucidated with infrared spectroscopy. *Phys. Chem. Chem. Phys.* **2007,** *9*, 3804-3817.
41. Martens, J.; Berden, G.; Gebhardt, C. R.; Oomens, J. Infrared ion spectroscopy in a modified quadrupole ion trap mass spectrometer at the FELIX free electron laser laboratory. *Rev. Sci. Instrum.* **2016,** *87*, 103108.
42. Munshi, M. U.; Berden, G.; Martens, J.; Oomens, J. Gas-phase vibrational spectroscopy of triphenylamine: the effect of charge on structure and spectra. *Phys. Chem. Chem. Phys.* **2017,** *19*, 19881-19889.
43. Berden, G.; Derksen, M.; Houthuijs, K. J.; Martens, J.; Oomens, J. An Automatic Variable Laser Attenuator for IRMPD Spectroscopy and Analysis of Power-dependence in Fragmentation Spectra. *Int. J. Mass Spectrom.* **2019,** *443*, 1-8.
44. Lemaire, J.; Boissel, P.; Heninger, M.; Mauclaire, G.; Bellec, G.; Mestdagh, H.; Le Caer, S.; Ortega, J.; Glotin, F.; Maître, P. Gas Phase Infrared Spectroscopy of Selectively Prepared Ions. *Phys. Rev. Lett.* **2002,** *89*, 273002.

45. Frisch, M. J.; Trucks, G. W.; Schlegel, H. B.; Scuseria, G. E.; Robb, M. A.; Cheeseman, J. R.; Scalmani, G.; Barone, V.; Petersson, G. A.; Nakatsuji, H., et al. *Gaussian 16, Revision A.03*, Gaussian, Inc.: Wallingford CT, 2016.
46. Pritchard, B. P.; Altarawy, D.; Didier, B.; Gibson, T. D.; Windus, T. L. A New Basis Set Exchange: An Open, Up-to-date Resource for the Molecular Sciences Community. *J. Chem. Inf. Model.* **2019,** *59*, 4814-4820.
47. Polfer, N. C. Infrared Multiple Photon Dissociation Spectroscopy of Trapped Ions. *Chem. Soc. Rev.* **2011,** *40*, 2211−2221.
48. Kesharwani, M. K.; Brauer, B.; Martin, J. M. L. Frequency and Zero-Point Vibrational Energy Scale Factors for Double-Hybrid Density Functionals (and Other Selected Methods): Can Anharmonic Force Fields Be Avoided? *J. Phys. Chem. A* **2015,** *119*, 1701-1714.
49. Grimme, S.; Ehrlich, S.; Goerigk, L. Effect of the Damping Function in Dispersion Corrected Density Functional Theory. *J. Comput. Chem.* **2011,** *32*, 1456-1465.
50. Grimme, S.; Antony, J.; Ehrlich, S.; Krieg, H. A Consistent and Accurate Ab Initio Parametrization of Density Functional Dispersion Correction (DFT-D) for the 94 Elements H-Pu. *J. Chem. Phys.* **2010,** *132*, 154104-154119.
51. Armentrout, P. B.; Yang, B.; Rodgers, M. T. Metal Cation Dependence of Interactions with Amino Acids: Bond Energies of Rb^+ and Cs^+ to Met, Phe, Tyr, and Trp. *J. Phys. Chem. B* **2013,** *117*, 3771-3781.
52. Dunbar, R. C. Complexation of Na^+ and K^+ to Aromatic Amino Acids: A Density Functional Computational Study of Cation-π Interactions. *J. Phys. Chem. A* **2000,** *104*, 8067-8074.
53. Dougherty, D. A.; Lester, H. A. The Crystal Structure of a Potassium Channel—A New Era in the Chemistry of Biological Signaling. *Angew. Chem. Int. Ed.* **1998,** *37*, 2329-2331.
54. Nakamura, R. L.; Anderson, J. A.; Gaber, R. F. Determination of key structural requirements of a K^+ channel pore. *J. Biol. Chem.* **1997,** *272*, 1011-1018.
55. Remko, M.; Fitz, D.; Broer, R.; Rode, B. M. Effect of metal Ions (Ni^{2+}, Cu^{2+} and Zn^{2+}) and water coordination on the structure of L-phenylalanine, L-tyrosine, L-tryptophan and their zwitterionic forms. *J. Molec. Model.* **2011,** *17*, 3117-3128.
56. Tomasi, J.; Mennucci, B.; Cammi, R. Quantum Mechanical Continuum Solvation Models. *Chem. Rev.* **2005,** *105*, 2999-3094.
57. Tapia, O.; Goscinski, O. Self-consistent reaction field theory of solvent effects. *Molec. Phys.* **1975,** *29*, 1653-1661.

Table 1. Relative Gibbs Energies at 298 K (kJ/mol) of Low-Lying $ZnCl(Phe)^+$ Complexes[a] ($CdCl(Phe)^+$ Complexes in Parentheses)[b]

Structure	B3LYP		B3P86		B3LYP-GD3BJ[c]		MP2	
[N,CO,π]	0.0	(0.0)	0.0	(0.0)	0.0	(0.0)	0.0	(0.0)
[N,CO]	0.7	(4.4)	8.9	(10.8)	22.0	(25.9)	28.6	(32.7)
[N,π]	19.3	(18.7)	20.7	(19.6)	29.1	(28.7)	22.6	(20.6)
[N,CO] (2)	14.6	(17.9)	24.2	(25.8)	37.0	(41.1)	43.3	(47.7)
[CO,π]	49.0	(44.2)	50.2	(44.9)	57.9	(53.5)	63.4	(57.9)
[CO,π] (2)	59.5	(57.3)	62.3	(60.4)	70.2	(68.3)	70.7	(70.4)
[CO]	113.1	(95.9)	131.3	(110.2)	146.9	(131.4)	160.9	(147.0)

[a]Calculated at the level of theory specified using a 6-311+G(2d,2p) basis set and B3LYP/6-311+G(d,p) geometries. [b]Calculated at the specified level of theory using a def2-TZVPP basis set and B3LYP/def2-TZVP geometries. [c]Calculated using B3LYP-GD3BJ optimized geometries (Zn, 6-311+G(d,p); Cd, def2-TZVP).

Table 2. Relative Gibbs Energies at 298 K (kJ/mol) of Low-Lying $ZnCl(Tyr)^+$ Complexes[a] ($CdCl(Tyr)^+$ Complexes in Parentheses)[b]

Structure	B3LYP		B3P86		B3LYP-GD3BJ[c]		MP2	
[N,CO,π]	0.0	(0.0)	0.0	(0.0)	0.0	(0.0)	0.0	(0.0)
[N,CO]	3.6	(7.7)	13.0	(14.6)	24.6	(27.9)	38.1	(40.6)
[N,π]	17.7	(19.6)	20.0	(20.7)	27.1	(27.3)	26.2	(25.8)
[N,CO] (2)	17.7	(22.0)	28.7	(30.7)	40.3	(43.9)	53.5	(57.0)
[CO,π]	43.1	(42.0)	43.4	(41.3)	51.7	(48.8)	58.6	(55.4)
[CO,π] (2)	57.4	(57.8)	68.5	(66.5)	60.4	(60.2)	71.8	(71.7)
[CO]	91.0	(77.3)	104.7	(86.4)	118.9	(105.7)	136.1	(122.4)

[a]Calculated at the level of theory specified using a 6-311+G(2d,2p) basis set and B3LYP/6-311+G(d,p) geometries. [b]Calculated at the specified level of theory using a def2-TZVPP basis set and B3LYP/def2-TZVP geometries. [c]Calculated using B3LYP-GD3BJ optimized geometries (Zn, 6-311+G(d,p); Cd, def2-TZVP).

Table 3. Relative Gibbs Energies at 298 K (kJ/mol) of Low-Lying $ZnCl(Trp)^+$ Complexes[a] ($CdCl(Trp)^+$ Complexes in Parentheses)[b]

Structure	B3LYP		B3P86		B3LYP-GD3BJ[c]		MP2	
$[N,CO,5\pi]_a$	0.0	(0.0)	0.0	(0.0)	0.0	[d]	0.0	(1.9)
$[N,CO,5\pi]_s$	1.7	(1.5)	2.3	(2.2)	2.3	(4.8)	2.2	(3.7)
$[N,CO,6\pi]_s$	7.0	(3.9)	7.4	(4.0)	2.7	(3.4)	14.5	(9.7)
$[N,CO,6\pi]_a$	6.6	(1.6)	7.8	(1.6)	4.4	(0.0)	12.7	(0.0)
$[N,6\pi]_s$	16.2	(17.6)	17.9	(18.6)	19.4	(24.7_4)	21.1	(20.2)
$[N,5\pi]_a$	12.4	(13.1)	16.4	(15.6)	20.2	(24.6_6)	23.9	(25.3)
$[N,CO]_s$	16.0	(13.4)	25.4	(19.7)	[e]	[e]	50.6	(43.9)
$[N,CO]_a$	13.3	(12.6)	23.2	(20.0)	33.1	(35,4)	52.3	(51.9)
$[CO]_a$	23.9	(12.4)	38.7	(21.6)	51.5	(44.5)	67.5	(54.4)
$[CO]_s$	25.1	(13.6)	39.3	(22.3)	51.7	(44.8)	66.3	(55.4)

[a]Calculated at the level of theory specified using a 6-311+G(2d,2p) basis set and B3LYP/6-311+G(d,p) geometries. [b]Calculated at the specified level of theory using a def2-TZVPP basis set and B3LYP/def2-TZVP geometries. [c]Calculated from B3LYP-GD3BJ optimized geometries (Zn, 6-311+G(d,p); Cd, def2-TZVP). [d]Collapsed to the $[N,CO,6\pi]_a$ geometry. [e]Collapsed to the $[N,CO,6\pi]_s$ geometry.

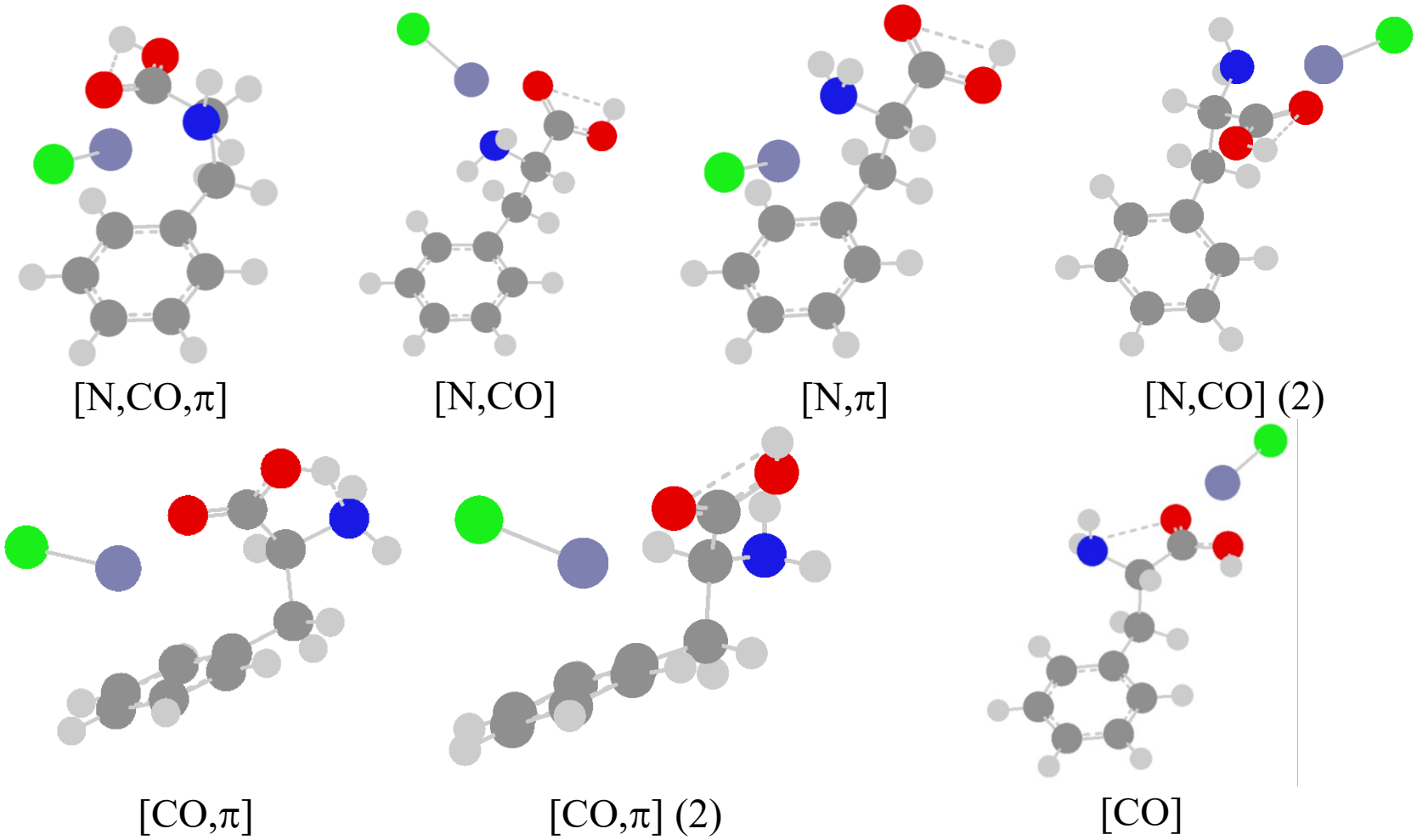

Figure 1. Structures of explored $ZnCl(Phe)^{+}$ conformers calculated at the B3LYP/6-311+G(d,p) level of theory. Dashed lines indicate hydrogen bonds. Red—oxygen, grey—carbon, white—hydrogen, blue—nitrogen, pale blue—zinc, green—chlorine.

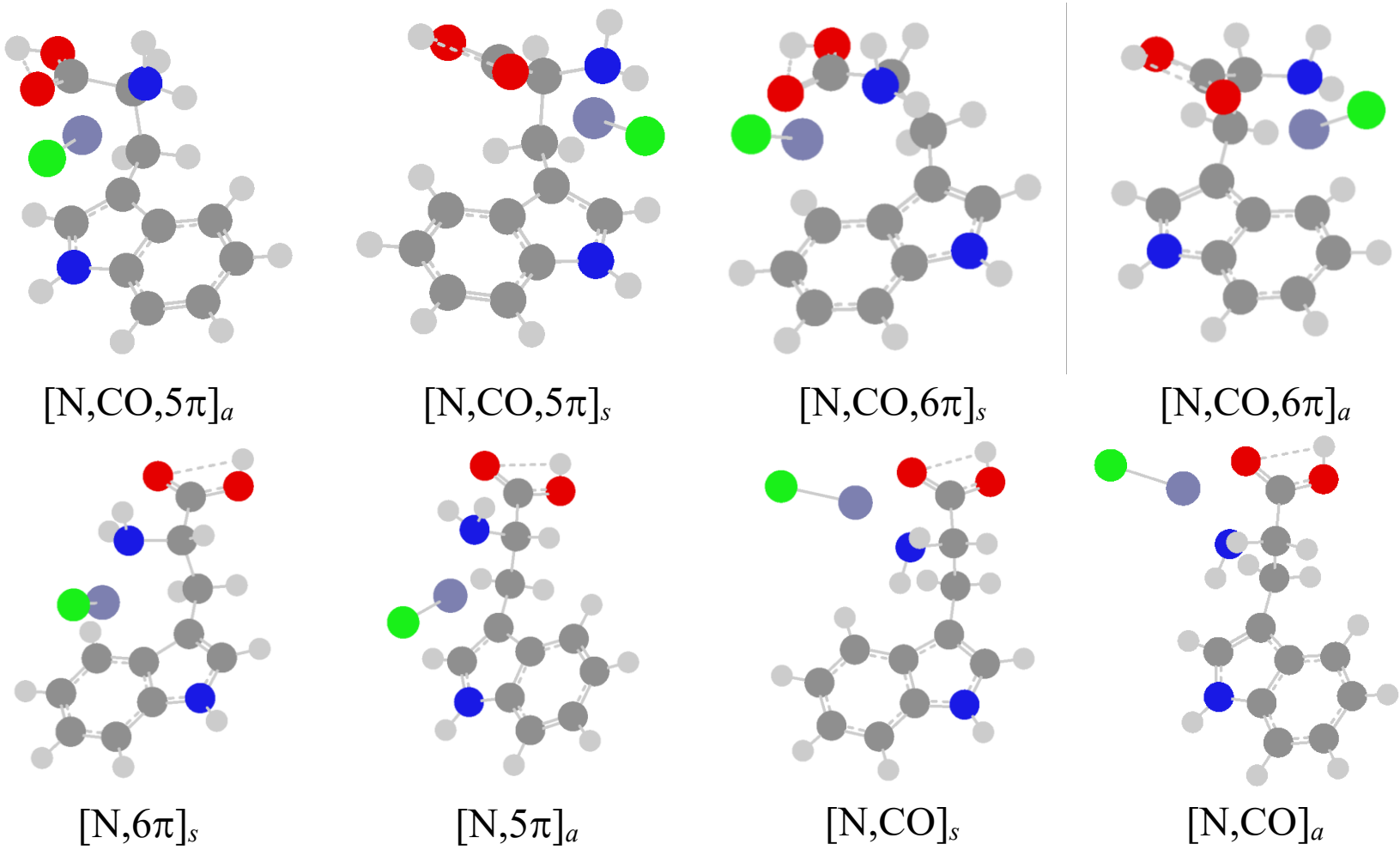

Figure 2. Structures of select $ZnCl(Trp)^+$ conformers calculated at the B3LYP/6-311+G(d,p) level of theory. Red—oxygen, grey—carbon, white—hydrogen, blue—nitrogen, dark blue—zinc, green—chlorine.

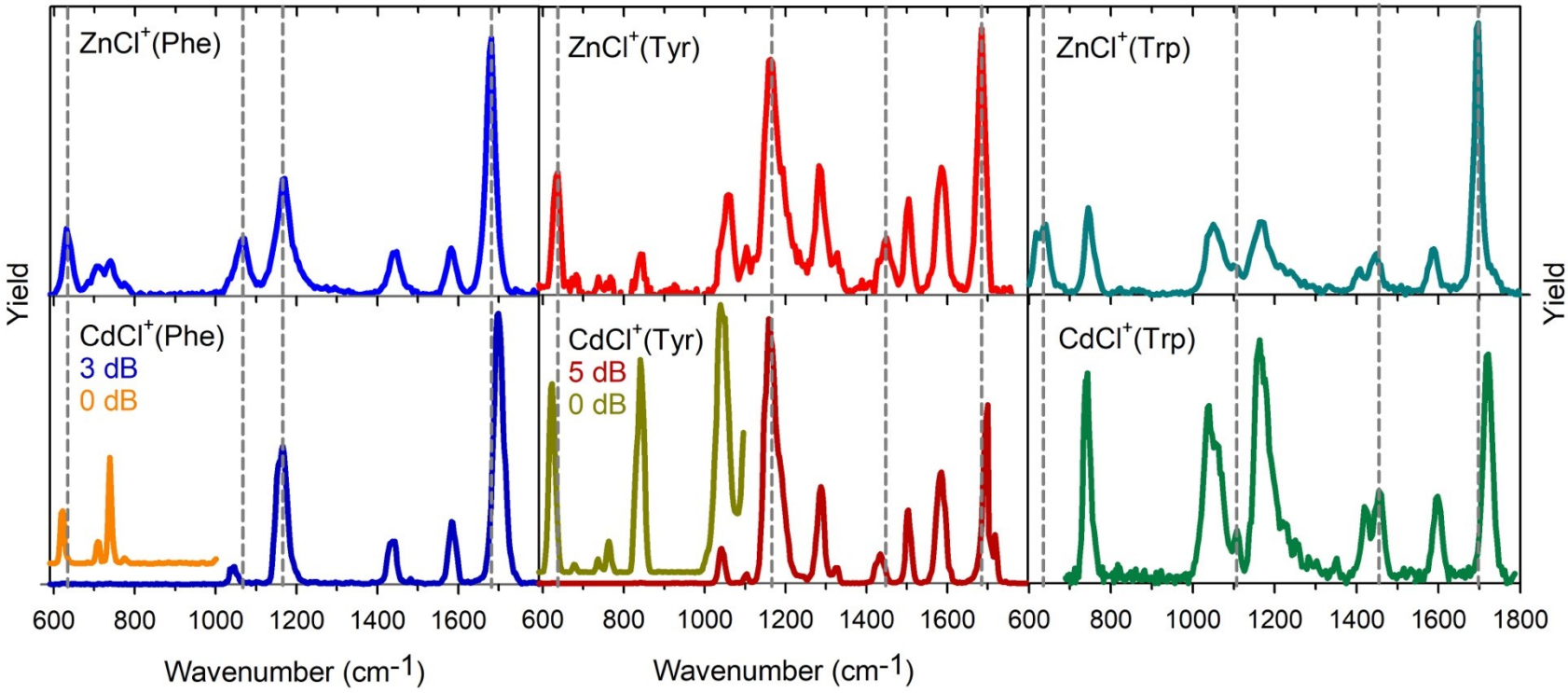

Figure 3. Comparison of the metal-chloride aromatic amino acid IRMPD action spectra, including experimental spectrum of $CdCl(Trp)^+$ from Dunbar and coworkers.[33] Vertical dashed lines mark peaks to facilitate the comparison of shifts. Spectra taken with attenuated FEL power are marked by color in their respective panel.

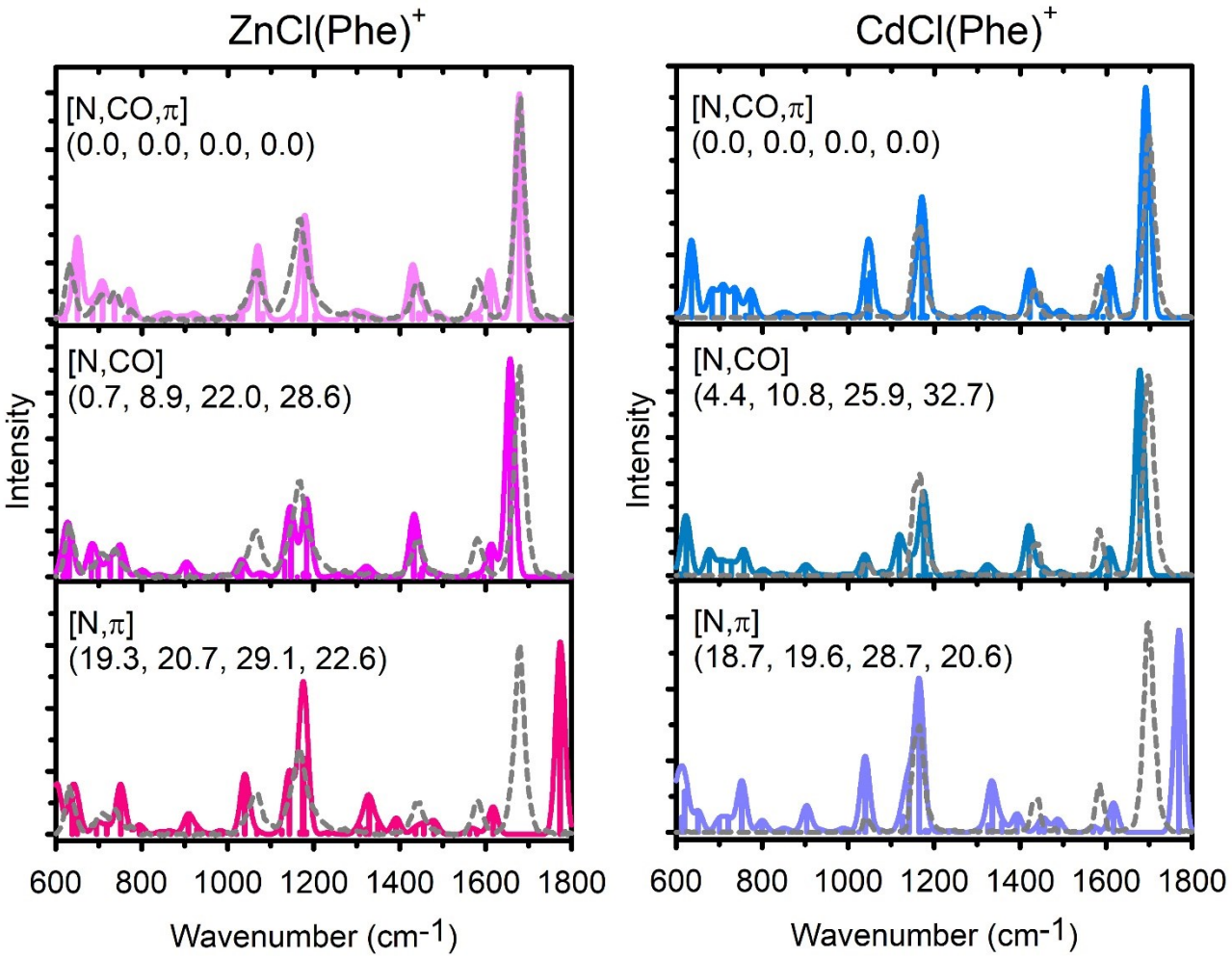

Figure 4. Comparison of the $MCl(Phe)^+$ experimental IRMPD action spectrum, shown here as the light grey dashed line, with IR spectra calculated at the B3LYP/6-311+G(d,p) (Zn) or B3LYP/def2-TZVP (Cd) level of theory for low-lying conformers. Relative 298 K Gibbs energies (kJ/mol) are listed at the B3LYP, B3P86, B3LYP-GD3BJ, and MP2 levels, respectively.

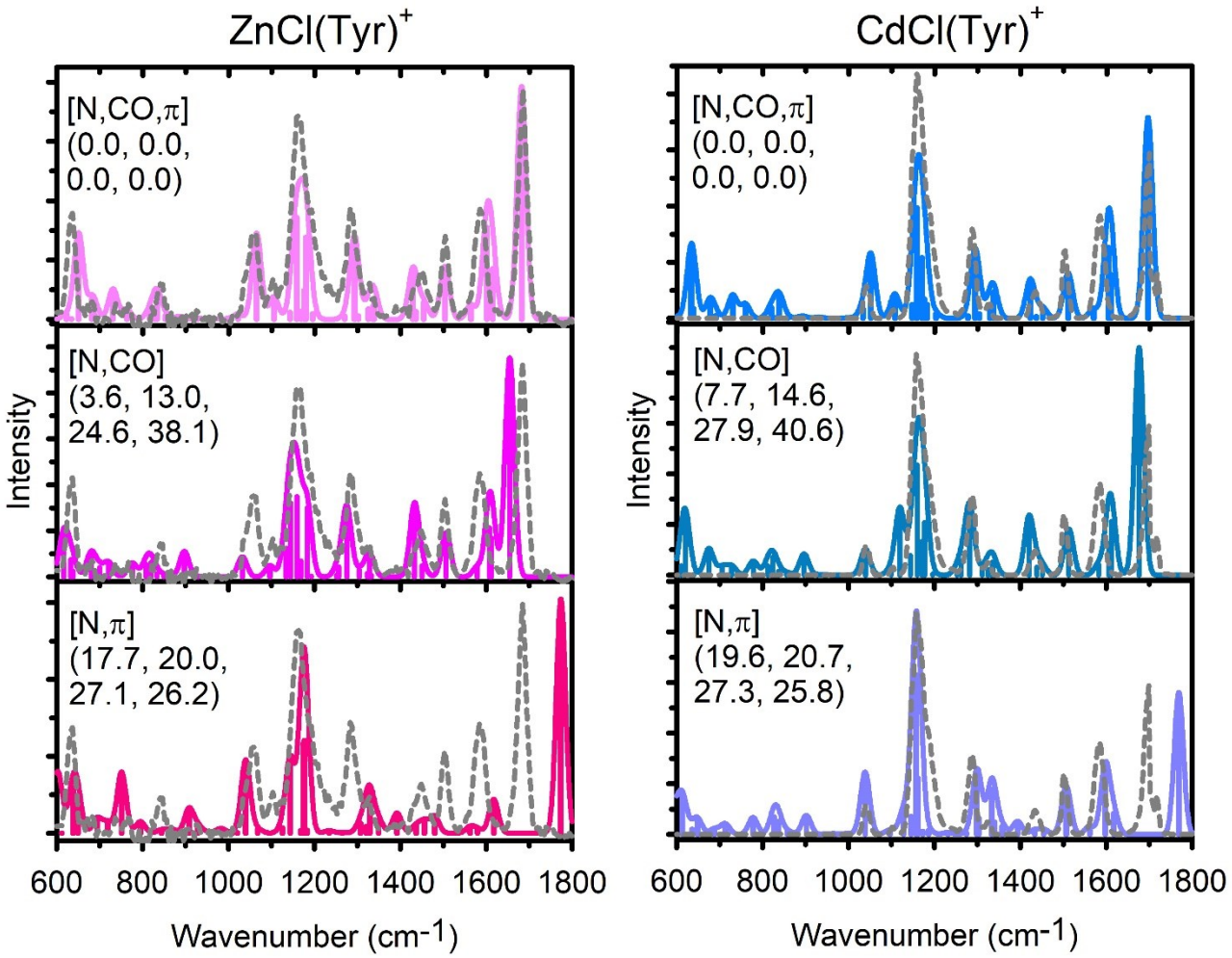

Figure 5. Comparison of the $MCl(Tyr)^+$ experimental IRMPD action spectrum, shown here as the light grey dashed line, with IR spectra calculated at the B3LYP/6-311+G(d,p) (Zn) or B3LYP/def2-TZVP (Cd) level of theory for low-lying conformers. Relative 298 K Gibbs energies (kJ/mol) are listed at the B3LYP, B3P86, B3LYP-GD3BJ, and MP2 levels, respectively.

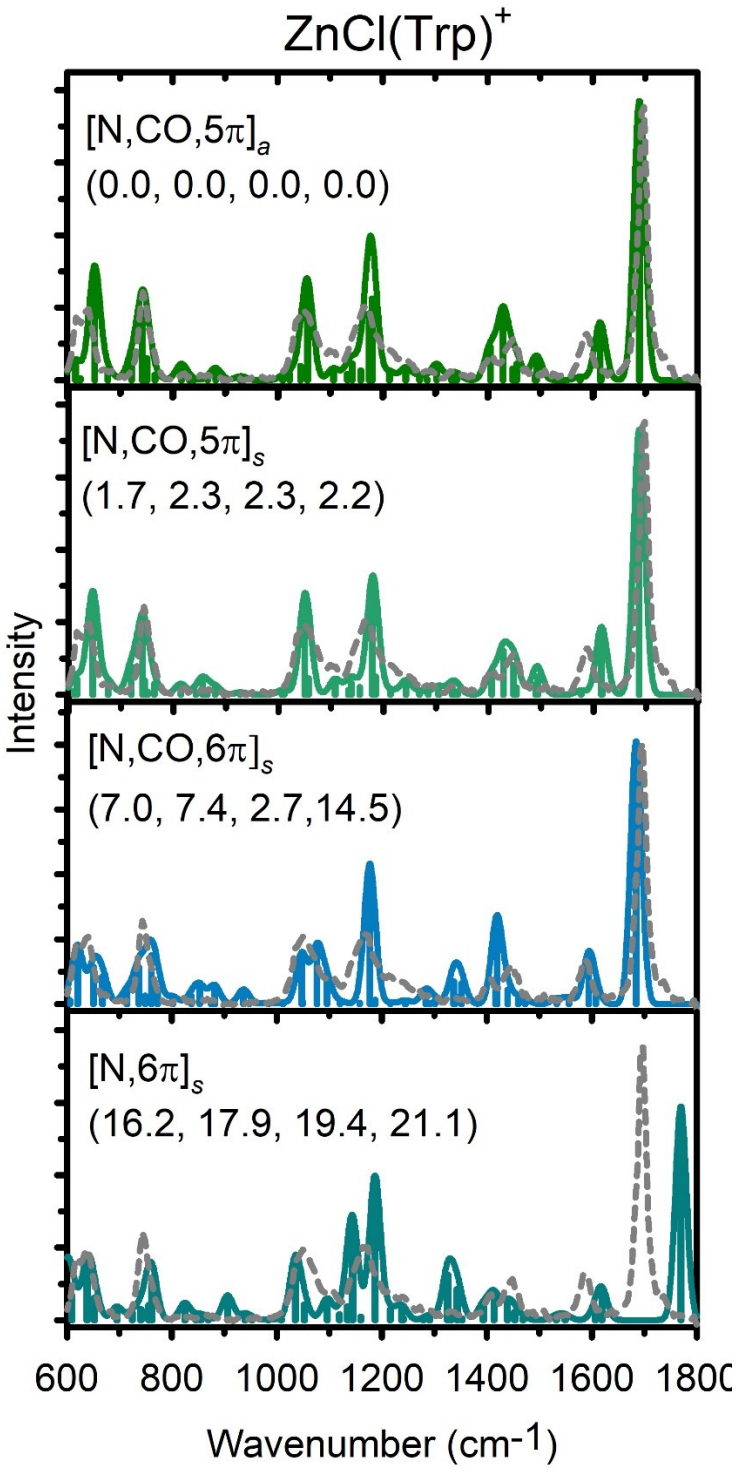

Figure 6. Comparison of the $ZnCl(Trp)^+$ experimental IRMPD action spectrum, shown here as the light grey dashed line, with IR spectra calculated at the B3LYP/6-311+G(d,p) level of theory for low-lying conformers. Relative 298 K Gibbs energies (kJ/mol) are listed at the B3LYP, B3P86, B3LYP-GD3BJ, and MP2 levels, respectively.

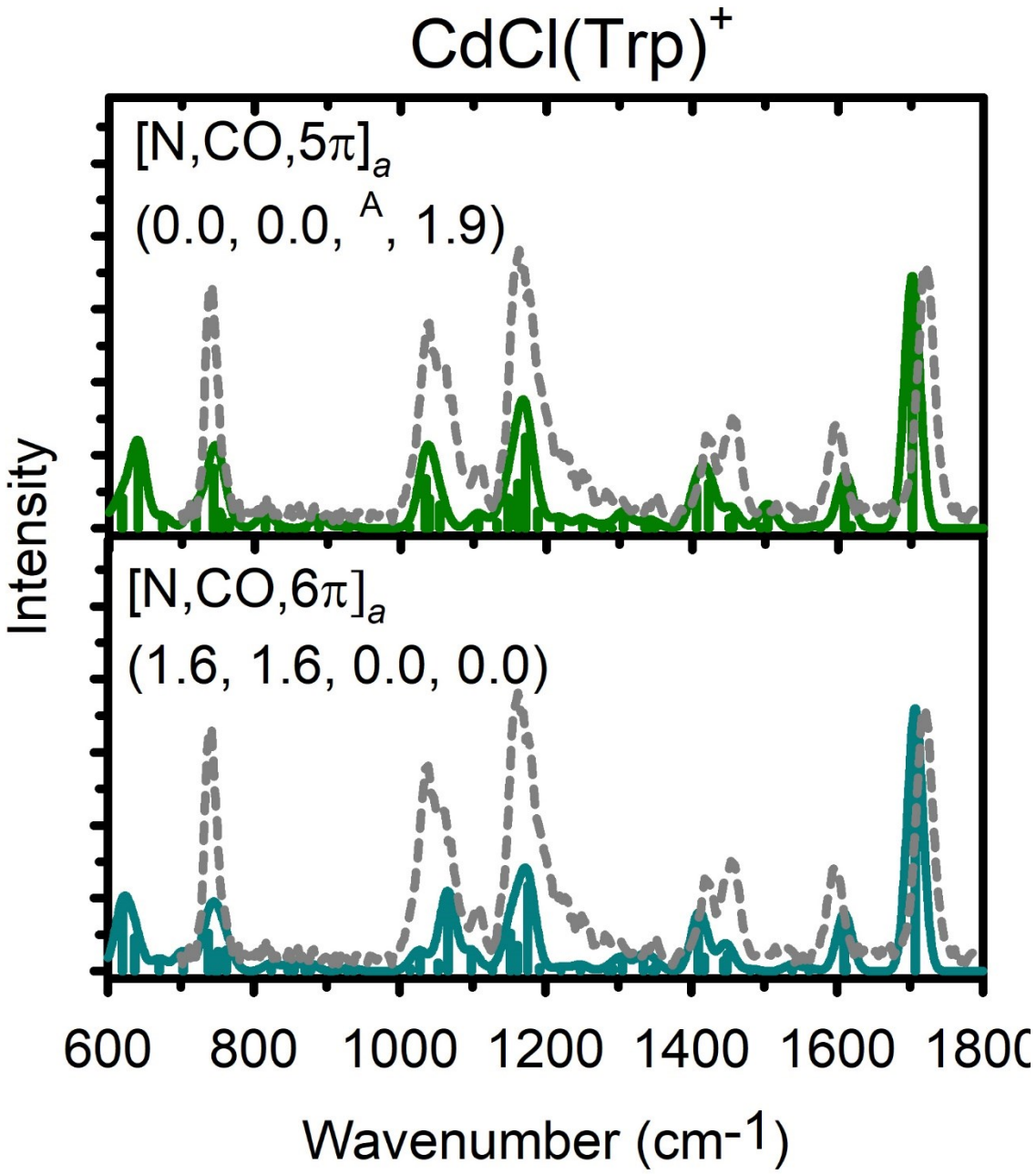

Figure 7. Comparison of the $CdCl(Trp)^+$ experimental IRMPD action spectrum from Dunbar and coworkers,[33] shown here as the light grey dashed line, with IR spectra calculated at the B3LYP/6-311+G(d,p) level of theory for two low-lying conformers. Relative 298 K Gibbs energies (kJ/mol) are listed at the B3LYP, B3P86, B3LYP-GD3BJ, and MP2 levels, respectively. [A] Collapsed to the $[N,CO,6\pi]_a$ geometry.

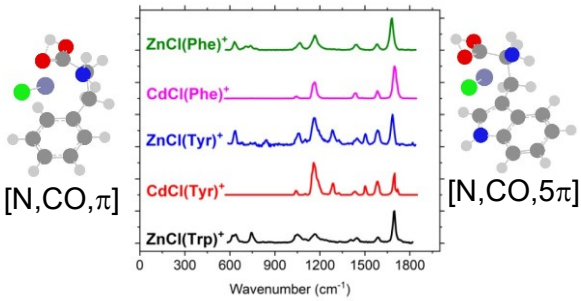
[N,CO,π]
ZnCl(Phe)+
CdCl(Phe)+
ZnCl(Tyr)+
CdCl(Tyr)+
ZnCl(Trp)+
0 300 600 900 1200 1500 1800
Wavenumber (cm-1)
[N,CO,5π]

TOC Graphic